Soft Matter

PAPER

View Article Online
View Journal | View Issue

Cite this: *Soft Matter*, 2014, **10**, 7630

Laterally structured ripple and square phases with one and two dimensional thickness modulations in a model bilayer system†

Ananya Debnath,‡[a] Foram M. Thakkar,§[a] Prabal K. Maiti,[b] V. Kumaran[a] and K. G. Ayappa*[a]

Received 12th May 2014
Accepted 30th July 2014

DOI: 10.1039/c4sm01031k

www.rsc.org/softmatter

Molecular dynamics simulations of bilayers in a surfactant/co-surfactant/water system with explicit solvent molecules show formation of topologically distinct gel phases depending upon the bilayer composition. At low temperatures, the bilayers transform from the tilted gel phase, $L_{\beta'}$, to the one dimensional (1D) rippled, $P_{\beta'}$ phase as the surfactant concentration is increased. More interestingly, we observe a two dimensional (2D) square phase at higher surfactant concentration which, upon heating, transforms to the gel $L_{\beta'}$ phase. The thickness modulations in the 1D rippled and square phases are asymmetric in two surfactant leaflets and the bilayer thickness varies by a factor of ~2 between maximum and minimum. The 1D ripple consists of a thinner interdigitated region of smaller extent alternating with a thicker non-interdigitated region. The 2D ripple phase is made up of two superimposed square lattices of maximum and minimum thicknesses with molecules of high tilt forming a square lattice translated from the lattice formed with the thickness minima. Using Voronoi diagrams we analyze the intricate interplay between the area-per-head-group, height modulations and chain tilt for the different ripple symmetries. Our simulations indicate that composition plays an important role in controlling the formation of low temperature gel phase symmetries and rippling accommodates the increased area-per-head-group of the surfactant molecules.

1 Introduction

Surfactants self assemble into a wide variety of thermodynamically stable and topologically distinct mesoscopic structures. The lamellar phase, which consists of alternating hydrophobic and hydrophilic leaflets made up of surfactants, is structurally similar to lipid bilayer membranes.[1] The lamellar phase can possess a wide spectrum of interesting structures which have been the subject of considerable theoretical and experimental research. Depending on the temperature, bilayer composition and hydration levels, the lamellar phase can exhibit morphologically different structures. Heating of the lamellar phase is associated with the well known gel to liquid crystalline transition, known as the main transition.[2]

Below this main transition, surfactants adopt various phases such as the gel (L_β), tilted gel ($L_{\beta'}$), subgel (L_c) and ripple ($P_{\beta'}$), depending on the orientation of the hydrocarbon tails and height modulations. Among these phases the ripple phase ($P_{\beta'}$)[3] has been the subject of extensive experimental and theoretical studies.

In lipid based bilayers, rippling of the lamellar phase is observed in the pre-transition region of the gel to liquid crystalline transition.[4,5] The factors that control the formation of the ripple, the associated microstructure and their symmetry have not been completely resolved. Experiments carried out with lipid bilayers indicate that the $P_{\beta'}$ phase can consist of symmetric or asymmetric 1D ripples depending on the thermal history.[6] There have been many theoretical models developed to explain the ripple phase by incorporating additional degrees of freedom in the elastic free energy below the main phase transition. The mechanism of the formation of the ripple phase has been studied by the interaction between the tilt order and membrane curvature.[7] The tilt arising from the two monolayers are proposed to be weakly coupled and the difference between the tilt order introduces an instability in the flat membrane phase.[8] In a different model, mutual interactions between the head group attraction and the chain packing are proposed to be responsible for the formation of the ripple phase.[9]

There have been few molecular simulations that reveal the formation of the 1D rippled phase. Using a united atom model (UA) for the dipalmitoylphosphatidylcholine (DPPC) lipid bilayer, Marrink *et al.*[10] reported an asymmetric sawtooth 1D

[a]*Department of Chemical Engineering, Indian Institute of Science, Bangalore 560012, India. E-mail: ayappa@chemeng.iisc.ernet.in*

[b]*Centre for Condensed Matter Theory, Department of Physics, Indian Institute of Science, Bangalore 560012, India*

† Electronic supplementary information (ESI) available. See DOI: 10.1039/c4sm01031k

‡ Current address: Indian Institute of Technology Jodhpur, Jodhpur 342011, India.

§ Current address: Shell India Markets Pvt. Ltd., Bangalore 560048, India.

ripple phase while cooling from a flat liquid crystalline phase. This sawtooth ripple phase consists of a non-interdigitated gel-like domain, characterized by a continuously changing tilt angle along the ripple vector and a fully interdigitated ($L_{\beta I}$) domain.[5] The formation of the ripple phase is found to be dependent on hydration and temperature. The interface between the two domains are fully disordered and significantly mobile. In a mesoscopic model of the lipid bilayer, the frustration of the head group surface area to the packing of hydrophobic tails leads to the formation of the 1D ripple, where the phases are dependent on the head–head repulsion parameter and the tail length.[11] The ripple phase has been found to occur if the head groups are sufficiently hydrated. Interestingly, the anomalous swelling is observed as a consequence of the conformational changes of the tails, but not directly due to rippling. Even in the absence of the ripple phase, anomalous swelling is found experimentally.[12] Using a Monte Carlo simulation with a coarse-grained lipid model, the structural properties of asymmetric and symmetric ripple states are compared[13] with those seen in experiments on phosphorylcholine (PC) lipids.[14] The model reproduces the experimental gel and fluid phase by modulating the head–head interaction potential in the presence of "phantom solvent" particles which interacts with the lipids. Using a dissipative-particle dynamics simulations, changes in enthalpy for saturated lipids are compared with differential scanning calorimetry experiments which show the formation of ripple phase.[15]

In contrast to the widely observed 1D ripple phase, the investigations on the 2D square phase are limited. The 2D square phase is characterized by rippling in two directions resulting in a topologically distinct egg carton shaped membrane structure. Although the 2D square phase was theoretically predicted by Chen *et al.* in 1995,[16] conclusive experimental evidence for the structure is still lacking. An X-ray diffraction study of saturated phospholipid molecules have shown the formation of a modulated 2D square lattice phase, which lies either between the L_β and L_α phase or between the $P_{\beta'}/L_{\beta'}$ and L_α phase depending on the temperature.[17] The origin of this phase is attributed to the coupling between variations in the local chain tilt to the bilayer shape. To the best of our knowledge this phase has not been reported as yet in realistic molecular simulations using atomistically resolved surfactant and water molecules and the microscopic origin of the 1D or 2D square phase is still not clearly understood. Using freeze-fractured electron microscopy, a tetragonal (square) phase was observed recently for cellular membranes obtained from extracted lipids.[18]

In this paper, we report the different phases obtained for bilayers made up of surfactant and co-surfactant molecules using all atom MD simulations. Understanding the various phases of mixed surfactant bilayers are important in the formulation of cosmetics, detergents as well as in secondary and tertiary oil recovery processes. In contrast to the well studied lipid bilayer systems, reports on mixed surfactant bilayers have not received much attention. Here we present simulations for bilayers made up of the cationic surfactants, behenyl trimethyl ammonium chloride (BTMAC) with co-surfactant, stearyl alcohol (SA) and illustrate that varying the membrane composition offers a flexible route to control the microstructure. The MD simulations of these mixed surfactant bilayers reveal a low temperature tilted $L_{\beta'}$ phase at a given BTMAC to SA ratio (0.33). With increasing BTMAC concentration, the tilted $L_{\beta'}$ phase can be transformed to the 1D $P_{\beta'}$ phase. A further increase in the BTMAC concentration transforms the 1D ripple to a rippled phase with 2D square symmetry. The atomistic perspective emerging from the MD study indicates that increasing the surfactant concentration induces specific headgroup areal spatial variations associated with a given ripple symmetry. The study suggests a compositional route which can be exploited to control and design membranes with desired structural functionalities. The organization of the paper is as follows, Section 2 describes the details of the simulation method, Section 3 describes the results for bilayers with different concentrations and temperatures. In Section 4 we discuss the results and in Section 5, we summarize our main results and conclude.

2 Simulation details

Simulations are performed for bilayers made up of the single tailed cationic surfactant BTMAC whose chemical formula is CH_3–$(CH_2)_{21}$–N^+Cl^-–$(CH_3)_3$ with the co-surfactant SA whose chemical formula is CH_3–$(CH_2)_{17}$–OH. The force-field parameters used for BTMAC and SA are similar to those used in our earlier study.[19] We carry out simulations with varying BTMAC to SA ratio at fixed water content. The different compositions investigated in the manuscript are shown in Table 1 and the bilayers increase in BTMAC content going from B1 to B2 to B3. Simulations are carried out for temperatures ranging from 283 to 330 K.

The initial configuration for the bilayers are constructed using the software PACKMOL.[20] Energy minimization of the initial structure is carried out with the steepest descent algorithm.[21] Our starting configurations for all bilayers are obtained from configurations equilibrated at 300 K (gel phase) with 0.5–2 ns long NVT simulations followed by 3 ns NPT simulations. We used the final configuration from the 300 K simulation as initial configurations for simulations at lower temperature, 283 K as well as for the simulations at higher temperatures. We have found that the generic state point for bilayers transforming into 1D/2D rippled phases are flat unit cells with box dimensions $\sim 4.5 - 6 \times 4.5 - 6 \times 7 - 8$ nm.

Table 1 Number of behenyl trimethyl ammonium chloride (BTMAC), stearyl alcohol (SA) and water molecules used in different bilayer compositions investigated. The ratio of BTMAC to SA are 1 : 2 in B1, 3 : 5 in B2 and 2 : 3 in B3. The percentage of BTMAC increases from B1 to B2 to B3

	Number of molecules				
Bilayer	BTMAC	SA	Water	BTMAC %	NPT (ns)
B1	296	600	16 000	0.33	32
B2	360	592	16 000	0.378	32
B3	400	600	16 000	0.4	32

After 3 ns NPT runs of unit cells at different temperatures, all bilayers are replicated twice both in the x and y directions to obtain the system size (box dimensions $\sim 12 \times 12 \times 8$ nm) in this paper. Next, all bilayers, B1, B2 and B3 are simulated for 32 ns in NPT ensemble at 1 bar. The results shown in the paper are analyzed for configurations of 4001 frames over 8 ns production runs. To further confirm the stability of low temperature phases obtained in this work, all three bilayers are simulated at 283 K for an additional 100 ns long run where all three low temperature phases were found to be stable and did not alter the results obtained with the shorter 8 ns runs. To investigate the system size effect further for the bilayer B3, where we obtained a square phase, a larger bilayer containing 900 BTMAC and 1350 SA molecules (box dimensions are $\sim 18 \times 18 \times 8$ nm) by replicating the unit cell square phase (box dimensions $\sim 6 \times 6 \times 8$ nm) was found to be stable at 283 K. Fig. S1 in ESI† shows the thickness modulations of the larger system in two directions confirming the presence of a 2D ripple. The thickness modulations in the square phases for the larger system differ by a factor of ~ 2 between maximum and minimum. However, an atomistic simulation starting from a flat bilayer having compositions mentioned in Table 1 (box dimensions $\sim 12 \times 12 \times 8$ nm) did not always result in the $P_{\beta S'}$ phase. This indicates that the $P_{\beta'}$ and $P_{\beta S'}$ phases cannot be easily stabilized and require careful preparation of the initial configurations.

The Berendsen thermostat is used to maintain the temperature, and the Berendsen semi-isotropic pressure coupling method[22] is used to maintain the zero interfacial tension by using same magnitudes for the diagonal components of the stress tensor. A time step of 2 fs is used for all simulations. Coulombic and van der Waals interactions are cut-off at 1.3 nm. Long-range electrostatic interactions are computed using the particle-mesh Ewald method with a 0.12 nm grid size. Periodic boundary conditions are applied in all three directions. Trajectories are collected every 2 ps. All simulations are performed with GROMACS-3.3.2.[23,24]

The surfactant co-ordinates are analyzed using the procedure given below to obtain the headgroup surfaces, bilayer thickness and Voronoi diagrams, head-to-tail distances and tilt vector.

• For every surfactant molecule, the tail-to-head vector $\mathbf{r}_{th}$ is defined as,

$$\mathbf{r}_{th} = \mathbf{r}_h - \mathbf{r}_t, \tag{1}$$

where $\mathbf{r}_h$ and $\mathbf{r}_t$ are the vector positions of the head and the last tail bead of the surfactant molecules respectively. The tail-to-head distance, r_{th} is the modulus of $\mathbf{r}_{th}$.

• If the bilayer normal is $\mathbf{n}$, and the tail to head vector for each molecule is $\mathbf{r}_{th}$, then the tilt vector is defined as $\mathbf{m} = \mathbf{r}_{th} - (\mathbf{n}\cdot\mathbf{r}_{th})\mathbf{n}$ which is the projection of the tail to head vector $\mathbf{r}_{th}$ (eqn (1)) in a plane perpendicular to the bilayer normal.

• The tilt angle θ which is the angle formed between the vector $\mathbf{r}_{th}$ and bilayer normal $\mathbf{n}$ is,

$$\theta = \arccos(\mathbf{n}\cdot\mathbf{r}_{th}/|\mathbf{n}||\mathbf{r}_{th}|), \tag{2}$$

• The dot product of the vector, $\mathbf{r}_{th}^{(i)}$, with the bilayer normal, $\mathbf{n}$, is used to determine whether the lipid molecule, i, belongs to upper or lower leaflets denoted by L_u and L_l respectively. Hence,

$$\mathbf{n}\cdot\mathbf{r}_{th}^{(i)} > 0 \Rightarrow i \in L_u, \tag{3}$$

$$\mathbf{n}\cdot\mathbf{r}_{th}^{(i)} < 0 \Rightarrow i \in L_l. \tag{4}$$

• Delaunay triangulation is performed on sets L_u and L_l separately using the (x, y) coordinates of the headgroups during this operation. Interpolation of this triangulated surface on the regular $n_x \times n_y$ grid is carried out to obtain the surfaces $z_u(x, y)$ and $z_l(x, y)$ corresponding to the sets L_u and L_l respectively.

• The bilayer thickness $d(x, y)$ is obtained[25] from the two surfaces.

$$d(x, y) = z_u(x, y) - z_l(x, y) \tag{5}$$

and the mean position of the interface z_0 is defined as,

$$z_0 = \frac{1}{N}\sum_{i=1}^{N} z_h^{(i)}, \tag{6}$$

where N is the total number of surfactant molecules in both leaflets (L_u and L_l) and z_h^i is the z coordinate of the head group of the i-th lipid. In a similar manner, the mean interface for upper and lower leaflets can be given as

$$z_{u0} = \frac{1}{N_u}\sum_{i\in L_u} z_h^{(i)}, \tag{7}$$

and

$$z_{l0} = \frac{1}{N_l}\sum_{i\in L_l} z_h^{(i)}, \tag{8}$$

where N_u and N_l are the total number of surfactant molecules in L_u and L_l respectively.

• Surface plots of the interfaces, $z_u(x, y)$, $z_l(x, y)$ as well as the thickness $d(x, y)$ are examined to identify the presence of the ripple phase. The height fluctuations of the upper and lower bilayers are defined as,

$$h_u(x, y) = \langle z_u(x, y) - z_{u0}\rangle \text{ and } h_l(x, y) = \langle z_l(x, y) - z_{l0}\rangle. \tag{9}$$

Additionally, Fast Fourier Transform (FFT) of height fluctuations are performed to determine the spectral intensity, $h(q)$, wavelength and symmetry of the ripple.

• In order to examine the specific surface area per head group, a Voronoi diagram is constructed for each leaflet including the headgroup locations for both BTMAC and SA using MATLAB.

3 Results and discussions

3.1 Influence of composition

We first discuss the structure of bilayer B1. Fig. 1(a) presents the snapshot at 283 K in the x–z plane where the bilayer is in the tilted gel phase ($L_{\beta'}$). There is no evidence of rippling at this composition. The Voronoi diagram from the positions of the

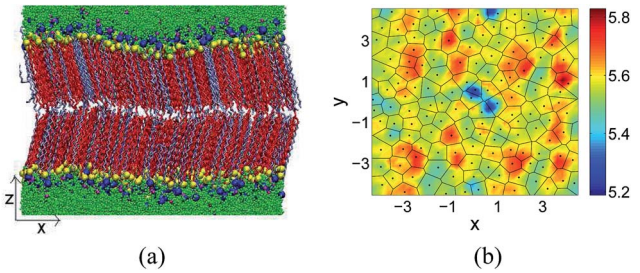

Fig. 1 (a) Snapshot for bilayer B1 at 283 K. The bilayer is a tilted flat bilayer in gel phase ($L_{\beta'}$). Color codes: iceblue – BTMAC tails, red – SA tails, green – water, magenta – Cl^-, yellow – oxygen (O^-), head group for SA, blue – nitrogen (N^+), head group for BTMAC. (b) Voronoi diagram of the area per head group superimposed on the thickness modulations of the upper leaflet of B1. Unit of the color bar is nm.

BTMAC and SA headgroups are superimposed on bilayer thickness, $d(x, y)$ (eqn (5)) for the upper leaflet as illustrated in Fig. 1(b). The trends are similar to those observed with the lower leaflet (not shown). The average thickness of the bilayer is 5.58 nm and the variations in the thickness are within 0.6 nm. The superimposed Voronoi diagrams show a relatively uniform area per head group across the bilayer consistent with the flat water-surfactant interface associated with the $L_{\beta'}$ phase.

We next present results for the bilayer B2 where the concentration of BTMAC is higher than that of B1 (Table 1). The snapshot in the y–z plane, shown in Fig. 2 (a) shows a periodic height modulation along the y axis. Two distinct regions are evident from the snapshot. The ripple consists of a thick non-interdigitated region where the lipid chains are extended in each leaflet. This is followed by a strongly interdigitated region of reduced thickness. There is a complex structure on either side of this interdigitated region which will be discussed below. The height maps of both the upper, $h_u(x, y)$ and lower, $h_l(x, y)$ surfaces (eqn (9)) are presented in Fig. 2(b). Both surfaces clearly show a 1D height modulation along the y direction, characteristic of the ripple phase. Fig. 2(c) shows the thickness modulations superimposed on Voronoi diagrams of area per head groups of upper surface. The area per head group correlates strongly with the thickness variation in the ripple, with the thickest (red) regions having a smaller area per head group when compared with the thinner (blue) regions in the bilayer. The area per head group on either side of the thin regions of the ripple are asymmetric with better packing along the positive y-directions as illustrated in Fig. 2(c). Fig. S2 in ESI† shows the thickness modulations $\left(d_x(y) = \frac{1}{N}\sum_{i=1}^{N} d_i(x,\ y)\right)$ of 1D ripple for B2 after averaging over the contours along the x-axis. The thickness has a minimum of about 3.13 nm corresponding to the interdigitated regions and a maximum of about 5.38 nm where the chains are extended and non-interdigitated. The ripple wavelength obtained from the thickness modulations is 5.7 nm. Fig. 2(d) shows the maps of the tail-to-head (or end-to-end) distances for both BTMAC and SA molecules superimposed on the Voronoi diagrams. Comparison of Fig. 2(c) and (d) clearly shows that the location of the minimum thickness regions do not correspond to surfactants with the minimum end-to-end distance. Instead the region of gentler height slope for the upper surface or the region of the steeper height slope for the lower surface (data not shown) corresponds to surfactants with a minimum tail-to-head distance and the highest area per head group. The region of minimum tail-to-head distances correspond to the high tilt and higher area per head group (see Fig. S3 in ESI†) lying in along a line bridging the thin and thick regions of the bilayer. Fig. S4(a) in ESI† shows that the tilt vector directs along the ripple axis (y). If we consider the configuration in Fig. 2, the transition from the minimum to maximum thickness region along the direction of increasing y takes place over a smaller lateral extent than the decrease back to the minimum thickness. This thin intermediate region corresponds to molecules in a highly defective state that bridges the interdigitated region of the bilayer on one leaflet with the subsequent non-interdigitated region. This situation also occurs on the lower leaflet, however this defective region is now shifted laterally by the extent of the interdigitated region. There is a complicated structure in regions of steeper height slope where the surfactants on one leaflet are still tilted, while there are relatively very few surfactants per head group on the other side, and the tails of the latter are in a disordered and highly coiled state. All of the above indicate the development of rather complicated correlations between height, head group density, tilt and tail conformation in order to accommodate the rippling in the bilayer.

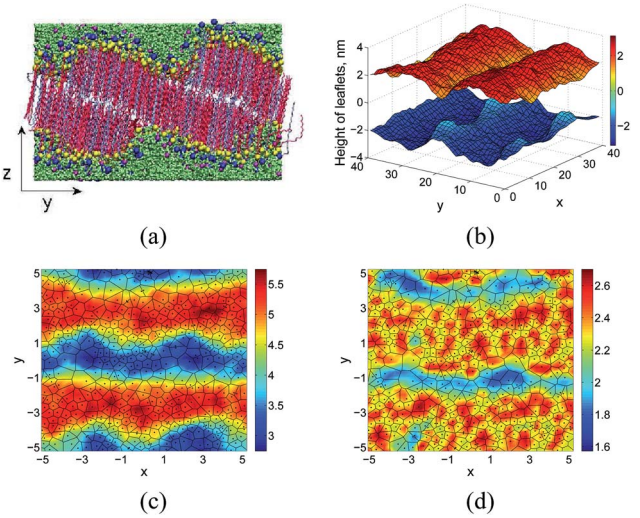

Fig. 2 (a) Snapshot for bilayer B2 at 283 K depicting the 1D ripple. Color codes: same as in Fig. 1(a). (b) Height fluctuations of upper and lower surfaces. For the clarity, the fluctuations for the upper and lower surfaces are shifted equally from their mean positions. (c) The contour of thickness modulations is superimposed on the Voronoi diagram of head groups of upper surface. (d) Voronoi diagram of the area per head group superimposed on the end-to-end distances of the surfactants on upper surface. The unit of all color bars in (b)–(d) is nm.

A similar combination of interdigitated and non-interdigitated regions with an intervening thin region of defective and highly tilted molecules has been observed in atomistic molecular simulations of DPPC by de Vries *et al.*[26] as well as in Monte Carlo simulations[13] using a coarse grained lipid model. In the atomistic simulations of de Vries *et al.*,[26] the

non-interdigitated regions were splayed out in their simulations, whereas we observe uniformly tilted, $L_{\beta'}$-like regions without any discernible splay between the two leaflets. In our system the two leaflets are well separated in regions of maximum height and the surfactant molecules have tilt and thickness similar to the $L_{\beta'}$ phase in Fig. 1.

Next, we study a bilayer with composition B3 (Table 1), in which the % of BTMAC is higher than that of B2. The snapshot of the bilayer B3 shown in Fig. 3 (a) along the y–z plane indicates the presence of a ripple similar to that observed in bilayer B2 (Fig. 2a). Fig. 3(b) shows the in-plane height variations for the upper and lower surfaces which is distinctly different from the 1D ripple observed in bilayer B2. The thickness map in Fig. 3(c) shows a distinct two-dimensional modulation in the thickness. The bilayer consists of two superimposed square lattices of maximum and minimum thicknesses with a period of about 5.34 nm. We refer to this phase as the 2D square ripple phase which is symmetric in both x and y directions. To our knowledge this is the first all atom simulation of this structure in bilayer membranes and we refer to this square phase as, $P_{\beta S'}$. Upon comparing Fig. 2(b) and 3(b), the amplitudes of the maximum and minimum thickness are similar for the 2D ripple when compared with the 1D rippled phase. The tail-to-head distance (r_{th}) of the surfactant molecules are shown in Fig. 3(d). The molecules with the shortest tail-to-head distance or equivalently those with the highest tilt (Fig. S3 in ESI†) do not coincide with the regions of minimum thickness. Instead these molecules with high tilt angles (35–60°) are associated with a few molecules in the region of gradual slope directed toward the point of minimum thickness. These molecules of high tilt also form a square lattice shifted from the square lattice associated with the thickness minima. In contrast, molecules of low tail-to-head distance or high tilt appear along a line in the transition between the regions of low and high thickness (Fig. 2c and d) for bilayer B2 in the 1D ripple case. When compared with the 1D rippled phase, molecules in the regions of maximum height, which corresponds to the $L_{\beta'}$ phase appear to have a slightly smaller tilt in the 2D ripple phase at 283 K (Fig. S3 in ESI†).

We further confirm the symmetry associated with the B2 and B3 bilayer by carrying out an FFT on the height co-ordinates (shown in Fig. S5 in ESI†). The spectral intensity for $h_u(q)$ obtained from $h_u(x, y)$ is plotted in the $q_x - q_y$ plane for both bilayers B2 and B3 (Fig. 4). For B2 we obtain two distinct peaks at 283 K along the y axis confirming a single wavelength associated with the 1D ripple for B2 (Fig. 4). The corresponding wavelength of the ripple is 5.62 nm. The spectral intensity for B3 shown in Fig. 4(c), verifies the presence of the square phase with four distinct intensity spots for the bilayer B3 at 283 K, indicating the presence of two equivalent wavelengths associated with the modulated square phase. The wavelength associated with the symmetric 2D ripple is 5.61 nm.

3.2 Influence of temperature

We observe interesting changes in the bilayer structure as the temperature is increased. The snapshots for both bilayers, B2 and B3, are shown in Fig. 5 at selected temperatures. At 283 K the bilayer B2 has a 1D ripple while B3 has a 2D ripple phase as illustrated in the previous section. Fig. 6 illustrates the height

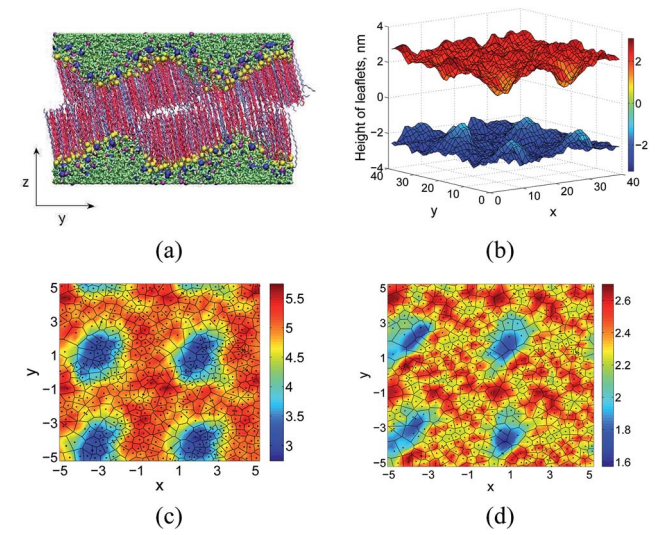

Fig. 3 (a) Snapshot of the bilayer B3 at 283 K. Color codes: same as in Fig. 1(a). (b) The height fluctuations of upper and lower surfaces for B3. For the clarity of the figure, the fluctuations for the upper and lower surfaces are shifted equally from their mean position. (c) Contour map showing the thickness fluctuations with the Voronoi area per head group of the upper surface. (d) The Voronoi of the area per head group is superimposed on the contour map of the end-to-end distances of the tails present in the upper surface. The unit of all color bars in (b)–(d) is nm.

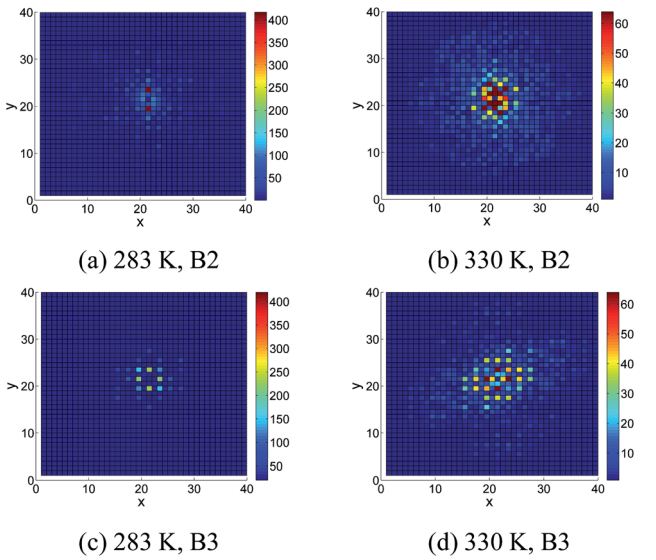

Fig. 4 Spectral intensity of height fluctuations of the upper surface from top view for bilayer B2 ((a) and (b)) and for B3 ((c) and (d)) as a function of grids along x and y. The intensity is plotted at 283 K and 323 K for two bilayers. There are two red spots at 283 K for B2 confirming two peaks associated with one ripple wave vector. For B3, there are four spots showing four peaks which confirm the presence of two wave vectors associated with ripple along x and y. The sharp peaks at lower temperature are merged at higher temperature.

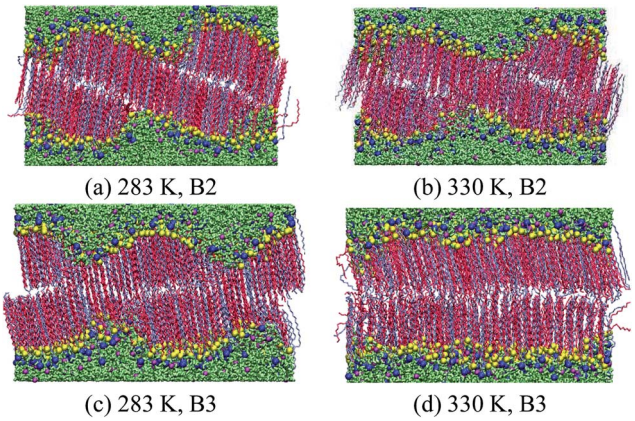

Fig. 5 Snapshots for bilayer B2 and B3 at two temperatures; 283 K and 330 K. The bilayer is in ripple phase between 283 K and 323 K. For B2 the ripple is slowly disrupted at 330 K before chain melting and becomes a flat bilayer. For B3 the ripples along two directions disappear slowly from 323 K and at 330 K, just before the chain melting, which leads to the formation of a flat bilayer. Color codes: same as in Fig. 1(a).

variations in both upper and lower leaflets at two temperatures for the 1D ripple bilayer. The 1D ripple with the height modulation in the *y*-direction persists to 323 K (data not shown). At 330 K the 1D ripple is only partially present and the bilayer is still in the gel phase although examination of the snapshots (Fig. 5) indicates greater disorder in the surfactant tails when compared with the structure at 283 K. The disruption in the 1D height modulation is evident when examining the height maps superimposed with the Voronoi diagrams as shown in Fig. 7(b) at 330 K. Although height undulations are still present, the 1D symmetry is clearly absent.

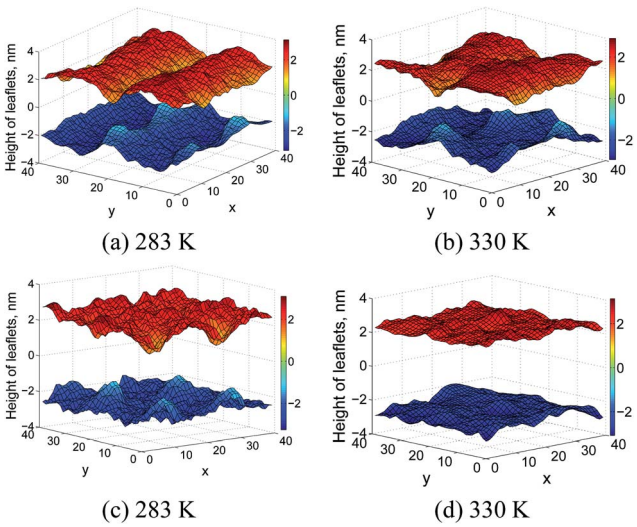

Fig. 6 (a) and (b) Height fluctuations of leaflets of bilayer at two temperatures for B2. The plots indicate that there is an associated wavelength along *x* direction which slowly disappears as temperature increases. (c) and (d) Height fluctuations of leaflets of bilayer at two temperatures for B3. For the clarity, the fluctuations for the upper and lower surfaces are shifted equally from their mean positions. The unit of all color bars in (a)–(d) is nm.

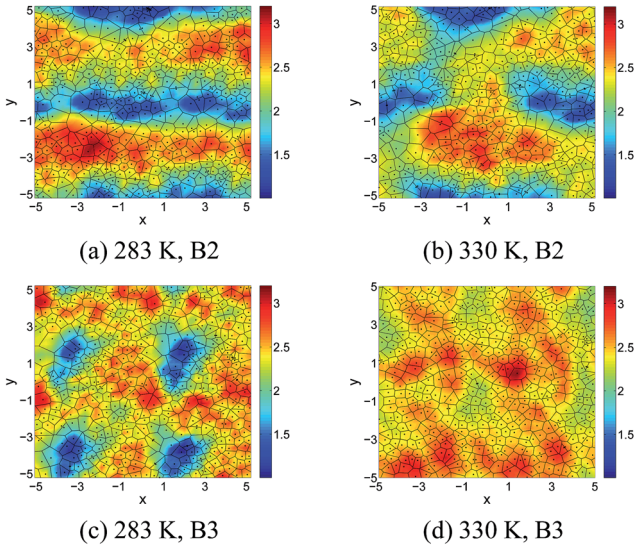

Fig. 7 Voronoi diagram of the area per head groups in the upper leaflet of bilayer B2 and B3 at two temperatures (283 K and 330 K) on the contour of their height. The plot shows that the area for the regions with lower height is higher indicating the ripple vector along that direction. The ripple disappears when the temperature is increased. The unit of all color bars in (a)–(d) is nm.

In our previous study of the melting transition of BTMAC/SA surfactant bilayers[19] we studied the melting transition with compositions similar to the B1 and B3 bilayers investigated in this study. However, the number of surfactants were about 4 times smaller than that used in this work. Hence we were unable to capture the low temperature 2D symmetry associated with the B3 bilayer. The transition from the low temperature gel phase to the L_α phase was found to occur above 330 K and at 338 K both bilayers with compositions similar to B1 and B3 were in the L_α phase.[19] Since the focus was on the low temperature phases in this study, we have not heated the bilayers to complete melting. From an examination of the snapshots (Fig. 5) both B2 and B3 bilayers are present in the gel phase at 330 K, consistent with our earlier work. The temperature dependence for the B3 bilayer is different from that of the B2 bilayer. The height fluctuations in Fig. 6(c) indicate that the 2D symmetry is preserved at 283 K. At 323 K there is a flattening of the bilayer leaflets (data not shown) and the 2D modulation is no longer observed at 330 K (Fig. 6 d). The absence of height undulations for B3 at 330 K is also confirmed in the height maps (Fig. 7) where the Voronoi diagrams indicate a relatively uniform area per head group in the bilayer leaflets. Thus bilayer B3 undergoes a transition from a 2D rippled phase to the $L_{\beta'}$ phase which is in the pretransition regime. Additional heating would result in melting the bilayer. At 330 K we do not observe signatures associated with melting, such as bilayer thinning and increase in area per head group, in either the B2 or B3 bilayers, further confirming that higher temperatures are required for the bilayers to melt. The snapshots at 330 K in Fig. 6 also indicate that the 1D ripple has greater thermal stability when compared with the 2D ripple.

The Fourier transforms of the heights also confirm the disappearance of the height modulated 2D ripple phase as the bilayer is heated to 330 K (Fig. 4b and d). However in the case of bilayer B2, weak height modulations are still present at 330 K. With increase in temperature of the B3 bilayer the four spots associated with the square phase collapse with few additional spots. The Fourier transform of thickness for bilayer B3 (shown in Fig. S5 in ESI†) shows four distinct peaks at low temperature, which broaden with temperature indicating a slow disruption of the modulation along x and y directions.

4 Discussion

It is well established that the different symmetries associated with the gel phase are driven by the head group packing as determined by the excluded volume of head groups. The influence of head group packing and head-head interaction, on the gel phase structure has been extensively studied for lipid molecules. Molecules with smaller head groups form the L_β phase where the chains are extended perpendicular to the bilayer normal. With increasing head group size, the molecules tilt to optimize the interaction between the chains and give rise to the $L_{\beta'}$ phase. A further increase in head group size or decrease in head–head interaction induces the $L_{\beta I}$ phase where the chains from opposing leaflets are interdigitated. Thus the symmetry of the gel phase can be controlled by several means; changing the molecule itself, altering head–head repulsion by moderating screening, adding a second small molecule component that predominantly partitions into the headgroup region, and altering the temperature. Some of these factors that control the gel phase structures have been illustrated in dissipative particle dynamics simulations by Krannenburg and Smit.[27] Lipid molecules that assemble into bilayers are always two tailed, in order to accommodate the unit ratio of hydrophobic projected area to the area of the head group required for the formation of the lamellar phase.[28] In the case of single tailed surfactant molecules which do not from bilayers by themselves, a co-surfactant is required to stabilize the bilayer as is the case with the BTMAC/SA system investigated in this study. Our simulations illustrate that altering the composition provides a convenient route to different gel phase symmetries. Since BTMAC has the larger head group area when compared with SA, increasing the BTMAC content in the bilayer induces the following sequence of gel phase structures as observed in our simulations at a fixed temperature of 283 K.

$$L_{\beta'} \rightarrow P_{\beta'} \rightarrow P_{\beta S'}$$

Since the rippled, $P_{\beta'}$ phase is formed between the gel to L_α transition, it is always observed between the $L_{\beta'}$ phase and the L_α phase. Hence tilting in the molecules is a requirement for the formation of the $P_{\beta'}$ phase and our observations are consistent with this sequence as a function of BTMAC composition. Since tilting optimizes inter-chain interactions, rippling provides an alternative mechanism for accommodating the increased area of head group (as a function of BTMAC) once tilting has been maximized. Fig. S4(a) and (b) in ESI† show that the tilt vector points along y axis for 1D ripple in B2. In contrast, the tilt vector in the square phase has a predominant component along gentler height slope of x axis in addition to a mild component along height slope of y axis. Thus, the chains will have more free space to tilt along two directions in the square phase accommodating the increased content of BTMAC. This indicates that rippling sets in once tilting has been maximized to accommodate the increase in BTMAC content. The 2D rippled phase provides an additional means to stabilize the structure as the BTMAC content is further increased. This phenomenon is first seen in the formation of the $P_{\beta'}$ phase which transforms into the 2D rippled, $P_{\beta S'}$ phase in the BTMAC/SA system. We also point out that the composition at which we observe the $P_{\beta S'}$ phase is near the phase boundary at which the bilayer to micelle transition occurs and 2D rippling could be a topological precursor to the formation of micelles in these systems.

5 Summary and conclusion

Using atomistic molecular dynamics simulations, we have studied structural changes in mixed surfactant bilayers as a function of membrane composition and temperature. At temperatures below the melting transition, the bilayers transform from the $L_{\beta'}$ phase to the 1D rippled, $P_{\beta'}$ phase as the BTMAC (cationic surfactant) concentration is increased. With further increase in the BTMAC concentration, we observe a novel 2D square phase with height modulations in two directions. Upon heating, this 2D phase transforms to the gel $L_{\beta'}$ phase. Rippling is seen as a mechanism to accommodate the increased area per head group of the BTMAC molecules once tilting has been maximized. Our simulations indicate that the low temperature symmetries in bilayers can be controlled by varying the composition. The surfactant-co-surfactant mixture is specifically interesting in this regard due to the larger area per head group and charge associated with one of the species, in this case the BTMAC molecule. The simulations reveal that the conformation required for accommodating these modulations in real systems is more complicated than those predicted by free energy functionals based on symmetry arguments. We observe a complex interplay between the thickness modulation, the area-per-head-group of the surfactant molecules and chain tilt. Although temperature has been widely used to determine the symmetry of the gel phase, our study indicates that membrane composition can be used for the formation of different phases in a controlled manner. This has implications in our understanding of biological membranes where lipid composition varies dynamically to control events occurring at the cell surface.

Acknowledgements

This work is carried out with a research grant from P&G Corporation USA. AD is thankful to IIT Jodhpur high performance cluster facility for computational work.

References

1 J. F. Nagle and S. Tristram-Nagle, *Biochim. Biophys. Acta, Gen. Subj.*, 2000, **1469**, 159.
2 D. F. Evans and H. Wennerstrom, *The Colloidal Domain Where Physics, Chemistry, Biology and Technology Meet*, VCH, New York, NY 10010, 1994.
3 A. Tardieu, V. Luzzati and F. C. Reman, *J. Mol. Biol.*, 1973, **75**, 711.
4 W. J. Sun, S. T. Nagle, R. M. Suter and J. F. Nagle, *Proc. Natl. Acad. Sci. U. S. A.*, 1996, **93**, 7008.
5 A. H. de Vries, S. Yefimov, A. E. Mark and S. J. Marrink, *Proc. Natl. Acad. Sci. U. S. A.*, 2005, **102**, 5392.
6 J. Katsaras, S. Tristram-Nagle, Y. Liu, R. L. Headrick, E. Fontes, P. C. Mason and J. F. Nagle, *Phys. Rev. E: Stat. Phys., Plasmas, Fluids, Relat. Interdiscip. Top.*, 2000, **61**, 5668.
7 W. Helfrich and J. Prost, *Phys. Rev. A: At., Mol., Opt. Phys.*, 1988, **38**, 3065.
8 U. Seifert, J. Shillcock and P. Nelson, *Phys. Rev. Lett.*, 1996, **77**, 5237.
9 P. A. Pearce and H. L. Scott, *J. Chem. Phys.*, 1982, **77**, 951.
10 C. Anzo, A. H. de Vries, H.-D. Hltje, D. P. Tieleman and S.-J. Marrink, *J. Phys. Chem. B*, 2003, **107**, 9424.
11 M. Kranenburg and B. Smit, *J. Phys. Chem. B*, 2005, **109**, 6553.
12 P. C. Mason, J. F. Nagle, R. M. Epand and J. Katsaras, *Phys. Rev. E: Stat., Nonlinear, Soft Matter Phys.*, 2001, **63**, 030902.
13 O. Lenz and F. Schmid, *Phys. Rev. Lett.*, 2007, **98**, 058104.
14 K. Sengupta, V. A. Raghunathan and J. Katsaras, *Phys. Rev. E: Stat., Nonlinear, Soft Matter Phys.*, 2003, **68**, 031710.
15 J. M. Rodgers, J. Sørensen, F. J.-M. de Meyer, B. Schiøtt and B. Smit, *J. Phys. Chem. B*, 2012, **116**, 1551.
16 C.-M. Chen, T. C. Lubensky and F. C. MacKintosh, *Phys. Rev. E: Stat., Nonlinear, Soft Matter Phys.*, 1995, **51**, 504.
17 L. Yang and M. Fukuto, *Phys. Rev. E: Stat., Nonlinear, Soft Matter Phys.*, 2005, **72**, 010901.
18 H. W. Meyer, W. Richter and J. Gumpert, *Biochim. Biophys. Acta, Gen. Subj.*, 1990, **1026**, 171.
19 A. Debnath, K. G. Ayappa, V. Kumaran and P. K. Maiti, *J. Phys. Chem. B*, 2009, **113**, 9183.
20 J. M. Martínez and L. Martínez, *J. Comput. Chem.*, 2003, **24**, 819.
21 A. R. Leach, *Molecular modelling: principles and applications*, Pearson Education Limited, Essex, England, 2001.
22 H. J. C. Berendsen, J. P. M. Postma, W. F. van Gunsteren, A. DiNola and J. R. Haak, *J. Chem. Phys.*, 1984, **81**, 3684.
23 H. J. C. Berendsen, D. van der Spoel and R. van Drunen, *Comput. Phys. Commun.*, 1995, **91**, 43.
24 E. Lindahl, B. Hess and D. van der Spoel, *J. Mol. Model.*, 2001, **7**, 306.
25 F. M. Thakkar, P. K. Maiti, V. Kumaran and K. G. Ayappa, *Soft Matter*, 2011, **7**, 3963.
26 A. H. de Vries, S. Yefimov, A. E. Mark and S. J. Marrink, *Proc. Natl. Acad. Sci. U. S. A.*, 2005, **102**, 5392.
27 M. Kranenburg and B. Smit, *J. Phys. Chem. B*, 2005, **109**, 6553.
28 J. N. Israelachvili, *Intermolecular and surface forces*, Academic Press Publications, Amsterdam, The Netherlands, 2011.